Virus Evolution, 2024, **10(1)**, veae098
DOI: https://doi.org/10.1093/ve/veae098
Advance Access Publication 20 November 2024
Research Article

Evolution of a novel engineered tripartite viral genome of a torradovirus

Massimo Turina[1,2], Luca Nerva[1,5], Marta Vallino[1], Niccolò Miotti[1], Marco Forgia[1], Marina Ciuffo[1], Bryce W. Falk[3], Inmaculada Ferriol[4,*]

[1]Department of Biology, Agriculture and Food Sciences, Institute for Sustainable Plant Protection, CNR, Strada delle Cacce 73, Turin 10135, Italy
[2]Department of Plant Protection, School of Agriculture, The University of Jordan, Amman, 11942, Jordan
[3]Department of Plant Pathology, UC-DAVIS, 1 Shields Ave, Davis, CA, 95616, United States
[4]Department of Plant Protection, Instituto de Ciencias Agrarias, ICA-CSIC,Calle Serrano 115 DPDO, Madrid, 28006, Spain

[5]Present address: CREA—Research Centre for Viticulture and Enology, Via XXVIII Aprile 26, 31 015 Conegliano, Treviso, Italy
*Corresponding author. Department of Plant Protection, Instituto de Ciencias Agrarias, ICA-CSIC, Calle Serrano 115 dpdo, Madrid 28006, Spain.
E-mail: iferriol@ica.csic.es

Abstract

Viruses in the *Secoviridae* include monopartite and bipartite genomes, suggesting the possibility to study members of this family to experimentally address evolutionary transitions resulting in multipartitism. Torradoviruses are bipartite members of the family *Secoviridae* characterized by a genus-specific 5′ open reading frame, named P21, encoded by RNA2. Here, in a study originally intended to verify if P21 can function *in trans*, we attempted to provide P21 from a third P21-expressing construct under control of the 35S promoter and containing the 5′- and 3′-untranslated regions (UTRs) of wild-type (WT) RNA2. When this construct was combined with an RNA2 with a complete deletion of the P21 coding region we verified that the P21 provided *in trans* cannot immediately complement the mutant, but occasional systemic infections in a limited number of the inoculated plants display the presence of a tripartite virus with an actively replicating P21-expressing RNA3. Furthermore, in all the systemically infected plants investigated in six distinct experiments, this replicating RNA3 accumulates deletions in a small region inside the original 3′-UTR provided by the cDNA clone. Such tripartite virus, which we obtained through deconstructing the coding potential of the RNA2 in two distinct RNAs, can be transmitted mechanically and by whiteflies, is competent for virion formation, and its RNA3 is encapsidated. It can be mechanically transferred for 11 serial passages without losing its infectivity or showing major genomic rearrangements. Furthermore, mixing equal amounts of WT and tripartite virus inocula in the same leaf resulted in plants systemically infected only with the WT virus, showing that the tripartite virus has lower fitness than the WT. To our knowledge, this is the first example of an engineered tripartite viral genome becoming stable through artificial evolution *in vivo*, in plants. This tripartite system was also used to derive a stable viral vector to express green fluorescence protein (GFP) systemically in the context of viral infection.

Keywords: torradoviruses; multipartite virus; evolution; *Secoviridae*

Introduction

Multipartite viruses have their genomes segmented into two or more nucleic acids and are encapsidated in separate virus particles which propagate independently. To complete the replication cycle, the presence of several particles in a single host cell is necessary, although there are experimentally demonstrated exceptions (Sicard et al. 2019). Recent advances in description of virus genome organizations have provided evidence of closely related viruses that exist either as monopartite or bipartite suggesting that such transition is widespread during virus evolution (Sicard et al. 2016, Lucía-Sanz and Manrubia 2017, Michalakis and Blanc 2020). Furthermore, the more detailed evolutionary history of viruses inferred from recent descriptions of the virosphere shows more and more examples of closely related monopartite viruses that have close relative bipartite viruses (Edgar et al. 2022, Neri et al. 2022). Some examples are the case of the genera *Closterovirus* and *Crinivirus* in the *Closteroviridae* family (Fuchs et al. 2020) or a mix of monopartite and bipartite genomes in the genus *Penicillimonavirus* in the *Mymonaviridae* families (Pagnoni et al. 2023). The evolutionary benefit of viral genome segmentation is an unsolved question in evolutionary biology. Some of the putative benefits of multipartite virus genome organization would be that smaller segments would have better tolerance to high mutation rates, faster replication, ability to exchange genetic information between different segments, or higher stability of viral particles (Sicard et al. 2016). On the contrary, multipartite genomes present specific challenges in coordinating the concomitant presence of genomic segments or their proteins in the newly infected plant cells (and new hosts)

in the right relative amounts (genome formula), and these aspects are currently being investigated in different experimental systems (Sicard et al. 2013, Bonnamy et al. 2024, Dall'Ara et al. 2024). Theoretical models about the evolutionary benefits and costs of multipartite genome organization are present in recent literature, but they still require further experimental validation (Zwart and Elena 2020, Leeks et al. 2023).

Artificial evolution is a powerful approach to experimentally address questions about multipartitism, specifically when deconstructing the coding potential of a single RNA segment in two or more segments. Viruses can be used as excellent tools for evolutionary studies because of their high mutation rates, rapid replication, and ability to efficiently enter host cells. This can involve techniques such as serial passaging, mutagenesis, and selection to accelerate the evolution of viruses towards a particular goal, such as increased infectivity or altered host range (Moya et al. 1995, Elena and García-Arenal 2023).

Members of the family *Secoviridae* (Order *Picornavirales*) are (+ sense) RNA plant viruses that have diverse genome architectures from monopartite to bipartite genomes (Fuchs et al. 2022). Seven of the genera have bipartite genomes (*Comovirus, Fabavirus, Nepovirus, Cheravirus, Sadwavirus, Torradovirus, and Stralarivirus*) and the other two genera are monopartite (*Sequivirus* and *Waikavirus*). The gene expression strategy of members of the family *Secoviridae* is to pack most coding capacities into large polyproteins which are subsequently proteolytically processed by one or two proteases (Mann et al. 2019, Fuchs et al. 2022).

Torradoviruses are single-stranded positive-sense bipartite viruses that separately encapsidate each genomic RNA in isometric particles (Sanfaçon et al. 2009, Fuchs et al. 2022). The RNA1 (∼7 kb) has one open reading frame (ORF) and codes for a polyprotein, which is proteolytically processed into functional proteins required for genome replication. The RNA1 can replicate independently of RNA2 (Ferriol et al. 2016b). The RNA2 (∼5 kb) has two ORFs encoding proteins required for virion assembly and movement. The RNA2-ORF1 codes for a protein of ∼21 kDa (P21) that is unique for torradoviruses and is required for systemic infection in tomato and *Nicotiana benthamiana* plants (Ferriol et al. 2018). The RNA2-ORF2 codes for a polyprotein which is processed by the 3C-like RNA1 protease into a movement protein and three capsid protein subunits (VP35, VP26, and VP24) (Ferriol et al. 2016a). Despite the recent emergence of new torradoviruses, the molecular biology of torradoviruses has not been well characterized. The role of torradovirus-encoded proteins in the infection cycle has been explored using different approaches such as expression vectors or infectious cDNA clones. Previously, we determined that the RNA1 of tomato apex necrosis virus (ToANV) is required for the replication and proteolytic processing of RNA2-encoded proteins (Ferriol et al. 2016a, 2016b) and the role of RNA2 P21 protein in long-distance movement in the infection cycle of ToANV (Ferriol et al. 2018). However, one unresolved question is the gene expression strategy of RNA2-ORF1 (P21) protein and whether this protein is a *cis*- or a *trans*-active element. In specific, knowing if a protein acts in *cis*-only or can act also *in trans*, helps design the experimental approach to study its biochemical role or the regulatory network it belongs to.

As part of further characterizing the functionality of P21, in this work we designed an experimental system to test if providing P21 *in trans* was sufficient to complement ToANV RNA2-ORF1 functional defective mutants. Complementation of the ToANV RNA2-ORF1 protein *in trans*, deconstructing the coding potential of the wild-type (WT) RNA2 in two distinct RNAs, lead to unexpected results that yielded a functional and stable tripartite ToANV through specific deletions in the 3′ untranslated region (UTR) that occurred *in vivo*. This newly derived stable tripartite torradovirus was used to engineer a new ToANV-based GFP vector capable of infecting systemically *N. benthamiana* plants.

Materials and methods

Plasmid constructs

Previously, a series of ToANV constructs derived from ToANV infectious cDNA clones were engineered to study the role of RNA2-ORF1 protein in ToANV infections (Ferriol et al. 2016b, 2018) and were used in this study. We generated two constructs that would not express the RNA2-ORF1 protein [R2-p21-sc and R2-Δp21, (Ferriol et al. 2018)] by using two different strategies: inserting three stop codons or engineering a deletion of 190 amino acids in the RNA2-ORF1 coding sequence (R2-p21-sc and R2-Δp21, respectively). In addition, we engineered a construct that will only express the RNA2-ORF1 protein and was flanked by the original RNA2 5′- and 3′-UTRs (R3-p21) (Ferriol et al. 2018).

To obtain an RNA2-ORF1 construct with synonymous mutations in the RNA2-ORF1 sequence, an inverse polymerase chain reaction (PCR) was performed using R3-p21 and the oligonucleotides ToANV-rectest-For/ToANV-rectest-Rev (Supplementary Table S1) using Phusion High-Fidelity DNA Polymerase (New England BioLabs) following manufacturer's instructions. The resulting plasmid was named R3-p21-rc.

To generate two constructs with 9-nt and 61-nt deletions in the 3′-UTR of the R3-p21 construct, two inverse PCRs were carried out using R3-p21 as a template and oligonucleotides Trip.A.For/Trip.A.Rev and Trip.B.For/Trip.B.Rev (Supplementary Table S1) using Phusion High-Fidelity DNA Polymerase (New England BioLabs) following manufacturer's instructions. The resulting plasmids were named R3-p21-TripA (9-bp deletion) and R3-p21-TripB (61-nt deletion). To engineer two constructs with 2415-nt and 2619-nt deletions within the RNA2, two inverse PCRs were carried out as described earlier. The construct R2-WT was used as a template, and the oligonucleotides used were ToANV-760Rev + ToANV-3175 F for construct R3-p21αβγ (2414-nt deletion) and ToANV-760Rev + ToANV-3379 F for construct R3-p21βγ (2618-nt deletion) (Supplementary Table S1).

To obtain an RNA3 that expressed GFP, we engineered a *Nco*I site in frame with the MP coding sequence, but just downstream of the termination of the RNA2-ORF1 coding sequence with an inverse PCR using Phusion High-Fidelity DNA Polymerase with oligonucleotides RNA2-ORF1-723 F (phosphorylated at its 5′ end) and RNA2-ORF1-*Nco*I-Rev (Supplementary Table S1) and using as template R3-p21-TripB. The resulting amplification product was digested with *Nco*I. A GFP fragment was amplified with oligonucleotides GFP-*Nco*I-F and GFP-*Sma*I-R (Supplementary Table S1) from a GFP encoding plasmid previously described (Crivelli et al. 2011) and digested with *Nco*I and *Sma*I. The two digested PCR products (vector and GFP insert) were ligated to obtain the plasmid R3-p21-TripB-GFP.

Agroinfiltration assays

Plasmids were transformed into *Agrobacterium tumefaciens* strain C58C1 cells and infiltrated into *N. benthamiana* or tomato line cv "York" as previously described (Ferriol et al. 2016b). Equal volumes of *A. tumefaciens* cells harboring the different constructs were mixed prior to infiltration and used at an optical density (OD) at 600 nm of 1.

Detection by DAS-ELISA

Double-antibody sandwich-enzyme-linked immunosorbent assay (DAS-ELISA) was carried out as previously described (Ferriol et al. 2018). Briefly, crude extracts from 0.5-cm disc diameter of plant leaf tissue were homogenized in 1 ml of PBS-Tween buffer containing 2% (w/v) poli vinil pirrolidona . Specific ToANV-anti-virion antibodies were used (Turina et al. 2007).

RNA purification and northern blot analysis

Total RNAs were extracted from 100 mg of plant tissue using RNeasy Plant Mini Kit (Qiagen). One microgram of total RNA was used for northern blot analysis using two ToANV probes (+ and – strands) that will hybridize to the 3′-UTR of ToANV RNA1 and RNA2 and all RNA2-derived constructs used in this work. Briefly, negative- and positive-strand probes were derived by cloning fragments of RNA2 in positive-strand and negative-strand direction in pGEMT-Easy (Promega Corp.). Two 257-bp probes (positions 4482–4738 in RNA2, Supplementary Fig. S4) were designed in a conserved region of the 3′-UTR of RNA2 and used to detect RNA1, RNA2, and RNA3 in both directions (+ and – strands). Northern blot analysis, probe synthesis, hybridization, and washes were performed as previously described (Ferriol et al. 2016b).

RT-PCR and sequencing

Sanger sequencing of recombinant and mutagenized plasmids and of purified reverse-transcriptase-PCR (RT-PCR) amplification products was carried out by Biofab Research (Rome, Italy). RT-PCR was carried out from total RNA extracted as detailed above; cDNA was synthesized with RevertAid First Strand cDNA Synthesis Kit (ThermoScientific) reverse transcription kit and PCR were carried out using OneTaq® DNA Polymerase reagents (NEB) using conditions previously detailed and oligonucleotides described in Supplementary Table S1 and in Ferriol et al. 2018.

Serial passages and competition experiments

For both experiments, *N. benthamiana* plants were grown in an insect-proof air-conditioned greenhouse (26°C ± 1°C) under natural light conditions. For the serial passage experiment, agroinfiltration was performed as above to obtain systemically infected plants. For each of the two treatments (WT and TripB), three plants were agroinfiltrated (R1-WT + R2-WT clones for WT and R1-WT + R2-Δp21 + R3-p21-TripB, for TripB, respectively). After the initial inoculation by agroinfiltration, a number of subsequent serial mechanical inoculations of plants dusted with carborundum were performed using as source of inoculum a mix of portions of three leaves for each treatment (1 g of fresh weight) from infected plants 10 dpi, homogenized using mortar and pestle in 5 ml of inoculation buffer (50 mM potassium phosphate buffer, pH 7, containing 1 mM Na-EDTA, 5 mM sodium diethyldithiocarbamate and 5 mM sodium thioglycolate) as previously detailed (Bertran et al. 2016). Serial inoculations were performed for 11 times and only one lineage was originated.

For the competition experiment, *N. benthamiana* plants were agroinfiltrated with mixed infections of two mixes of *A. tumefaciens* cells harboring the desired clones in equal amounts (each suspension 1OD): (i) WT: R1-WT+ R2-WT + pJL89 (empty vector) and (ii) Trip B: R1-WT + R2-Δp21 + R3-p21-TripB. As controls, single infections of WT and TripB were also performed. Systemically infected leaves were harvested 5 dpi and processed for northern blot analysis as described earlier.

Virion purification, western blot, and transmission electron microscopy observations

Virion purification was performed through differential centrifugation steps and sucrose gradients exactly as previously described (Turina et al. 2007). Sodium dodecyl sulfate–polyacrylamide gel electrophoresis (SDS–PAGE) and western blot analysis of purified preparations post-sucrose gradients were carried out as described previously in detail (Rastgou et al. 2009) using ToANV polyclonal antibodies raised against purified virions at 1:2000 dilution (Turina et al. 2007).

Transmission electron microscopy (TEM) observation of purified particles through negative staining with uranyl acetate was done as previously detailed (Ferriol et al. 2018). Electron dense and electron transparent particles were counted in different areas of TEM grids, reaching a total of about 600 viral particles.

RNA secondary structure analyses

The secondary structures of the 3′-UTRs of the RNA2 WT, R2-p21 and R2-p21-6bp-, R2-p21-9bp (TripA), and R2-p21-9bp (TripB)-derived RNAs were predicted using the Mfold program at the website (http://unafold.rna.albany.edu/?q=mfold/RNA-Folding-Form) (Zuker 2003), and illustrated with the RNA2Drawer program (Johnson et al. 2019).

Total RNA extraction and RNA-seq transcriptome assembly

Total RNAs were extracted using Total Spectrum RNA reagents (Sigma-Aldrich). RNAs were quantified using a NanoDrop 2000 Spectrophotometer (Thermo Scientific). One microgram of RNA pooled from equal amounts of three infected plants from each of the two treatments (WT and TRIP-B) were sent to sequencing facilities (Macrogen, Seoul, Republic of Korea). Ribosomal RNA was depleted (Ribo-ZeroTM Gold Kit, Epicentre), cDNA libraries were built with TrueSeq total RNA sample kit (Illumina) and sequencing was performed by an Illumina HiSeq4000 system generating paired-end sequences. Bioinformatic analyses of RNAseq raw reads were performed as previously described. BWA (0.5.9) (Li and Durbin 2009) and SAMtools (0.1.19) (Li et al. 2009) were used to map reads on reference sequences of the infectious clones and visualized with IGV (Thorvaldsdóttir et al. 2013). Only mutations present in >2% of the reads were scored.

Whitefly transmission experiments

All plants were grown in 10 cm diameter pots in a growth chamber at 26°C under a 14 h light regime or in insect-proof greenhouses under natural light conditions. *Trialeurodes vaporariorum* whiteflies from a population harvested from a greenhouse at the Turin botanical garden were maintained on melon plants in insect proof growth chambers at 26°C ± 1°C, with a 16:8 h (1ight-dark) photoperiod and passaged to new healthy plants every 2 weeks. Non-viruliferous *T. vaporariorum* whiteflies were then transferred to ToANV-WT or ToANV-TripB-infected *N. benthamiana* plants by gentle shaking as previously described and removed after an acquisition access period of 48 h (Ferriol et al. 2016b). For inoculation access, adult whiteflies were placed on receptor plants (*Physalis floridana* and *Nicotiana occidentalis*) in glass tubes (6 cm diameter, 12 cm high), topped with a nylon screen and after an inoculation access period of 72 h plants were sprayed with insecticide to remove whiteflies; after that plants were transferred back to the greenhouse and monitored for symptoms and for sample harvesting for 2 weeks.

GFP visualization

Nicotiana benthamiana leaves were agroinfiltrated with a combination of *A. tumefaciens* cells harboring R1-WT + R2-Δp21 + R2-p21-TripB-GFP and then examined for GFP fluorescence at 3 and 6-days post–agroinfiltration (dpa). Plants agroinfiltrated with R1-WT + R2-Δp21 + R2-p21-TripB were used as a negative control. Fluorescence was observed using a Leica M205 FA stereo microscope (Leica Microsystems, Wetzlar, Germany). A 488 nm Argon laser line and a window of 500–525 nm were used for excitation and for collection of the GFP signal, respectively. Pictures were captured using a ×10 or ×20 objective and processed (for trimming, contrast and brightness adjustment, and figure assembly) using the GNU Image Manipulation Program (https://www.gimp.org/).

Results

Providing P21 "*in trans*" to complement the P21 stop codon mutant results in delayed systemic infection requiring recombination events

Previously, we determined that the ToANV RNA2-ORF1 protein (P21) is required for systemic infection, but not for cell-to-cell movement, virion formation or replication in *N. benthamiana* plants (Ferriol et al. 2018). Such demonstration was based on mutants of agroinfectious clones: in this virus-inoculation approach, the viral RNA is synthesized in plant cells *in vivo* from a 35S promoter from binary plasmids carrying cDNA corresponding to viral RNA1 and RNA2 that are grown in *A. tumefaciens* cells; the agrobacterium suspension is infiltrated through pressure in intracellular spaces in the leaves ("agroinfiltration") and this process starts an infection that we previously showed cannot be distinguished from a WT virus mechanical inoculation. The two P21 constructs that were not able to express the RNA2-ORF1 protein were R2-p21-sc and R2-Δp21 (Fig. 1 and Table 1). The R2-p21-sc construct contained three stop codons in the RNA2-ORF1 coding sequence, whereas R2-Δp21 had a deletion corresponding to a cDNA region coding for 190 amino acids (almost the entire cDNA corresponding to the RNA2-ORF1 protein). Agroinfiltration experiments in *N. benthamiana* plants using R2-p21-sc and R2-Δp21 constructs in combination with R1-WT construct resulted in replication in inoculated areas, but an inability to infect systemically *N. benthamiana* and tomato plants (Ferriol et al. 2018).

In this work, we attempted to complement *in trans* the RNA2-ORF1 protein function by engineering a third construct that contained the RNA2-ORF1 protein coding sequence and the 5′- and 3′-UTRs of the RNA2-WT (R3-p21, Fig. 1). Agroinfiltration assays of the R3-p21 construct in combination with R1-WT and R2-p21-sc constructs in *N. benthamiana* plants resulted in 100% systemic infections, but there was a delay in symptoms appearance and virus presence with plants showing symptoms only 15 dpa, contrary to what happens with ToANV-WT constructs (R1-WT + R2-WT) where most of *N. benthamiana* plants were systemically infected at 4 dpa (Table 1). This could imply a lack of direct and immediate complementation *in trans* of the P21 null mutant. RT-PCR using specific primers to identify the R3-p21 and R2-p21-sc-derived RNAs (Supplementary Table S1) performed on total RNAs obtained from upper non-inoculated leaves of *N. benthamiana* agroinfiltrated with R1-WT + R2-p21-sc + R3-p21, revealed that the third RNA provided *in trans* by R3-p21 through agroinfiltration was not present in the systemically infecting viral progeny. Furthermore, the nucleotide sequence of R2-p21-sc had reverted to the WT sequence, thus eliminating the stop codons in the viral progeny (Supplementary Fig. S1).

To estimate whether those changes in the viral progeny were due to recombination between the R2-p21-sc- and R2-p21-derived RNAs (and not reversions in the three stop codon position or contamination events), we generated the construct R3-p21-rc (Fig. 1): an R3-p21-derived construct with a synonymous mutation at the amino acid G^5 (T to A at position 165; GGT to GGA accession KT756877) in the RNA2-ORF1 sequence that would allow us to monitor a possible recombination event. When we agroinfiltrated *N. benthamiana* plants with *A. tumefaciens* cells harboring R1-WT + R2-p21-sc + R3-p21-rc constructs, five out of five inoculated plants were systemically infected by 15 dpa. Sequencing of RT-PCR products corresponding to the mutated region of P21 from total RNAs of upper non-inoculated plants (three samples) confirmed the presence of the synonymous mutation in the sequence of the RNA2 demonstrating that a recombination event between the RNA2 derived from R2-p21-sc containing the stop codon mutations and the RNA expressed from R3-p21-rc gave rise to the restored progeny (Supplementary Fig. S2).

Providing P21 "*in trans*" to complement the R2-Δp21 deletion mutant results in occasional delayed systemic infection with a tripartite virus progeny

We next attempted to complement the RNA2-ORF1 deletion mutant (R2-Δp21) construct with our R3-p21 construct. *N. benthamiana* plants agroinfiltrated with R1-WT + R2-Δp21 + R3-p21 only became occasionally infected after 15 dpa (18% of inoculated plants from three experiments) (Table 1). Northern blot analysis of total RNAs from upper non-inoculated leaves of plants agroinfiltrated with the R2-Δp21 and R3-p21 constructs showed the presence of three RNAs of positive and negative sense, with sizes putatively corresponding to the RNA1-, RNA2-Δp21-, and RNA3-p21-derived replicating RNAs (Fig. 2). The presence of relatively abundant strand RNA corresponding to RNA3 demonstrates that complementation is not purely through systemic movement of the third RNA provided locally through agroinfiltration, but through active replication of this third RNA. Sequencing RT-PCR products for RNAs 1, 2, and 3 from total RNAs from the upper, non-inoculated leaves showed the absence of nucleotide changes in the R2-Δp21-derived RNAs, where the P21 coding sequence was deleted. However, there were deletions in the 3′-UTR of R3-p21-derived third RNA. Deletions of 6, 9, and 61 nt were present in the 3′-UTR of R3-p21-derived RNAs that accumulated in systemically infected plants; these deletions were obtained from three different *N. benthamiana* plants obtained in each of three different experiments (Fig. 3).

To investigate whether these deletions have any effect on the secondary structure of the 3′-UTR of each of the derived RNAs, we compared the predicted secondary structures using the MFold program. The predicted RNA secondary structures of the 3′-UTRs of R3-p21, R2-WT, and R3-p21-6bp-deletion showed similar RNA secondary structures. However, R3-p21-9bp-deletion and R3-p21-61bp-deletion-derived RNAs had different secondary structures when compared with R3-p21 and R2-WT (Supplementary Fig. S3). In addition, multiple nucleotide alignment of the RNA1 and RNA2 3′-UTRs of different tomato marchitez virus (ToMarV) isolates showed that these deletions are not present in other ToMarV naturally occurring isolates (Supplementary Fig. S4).

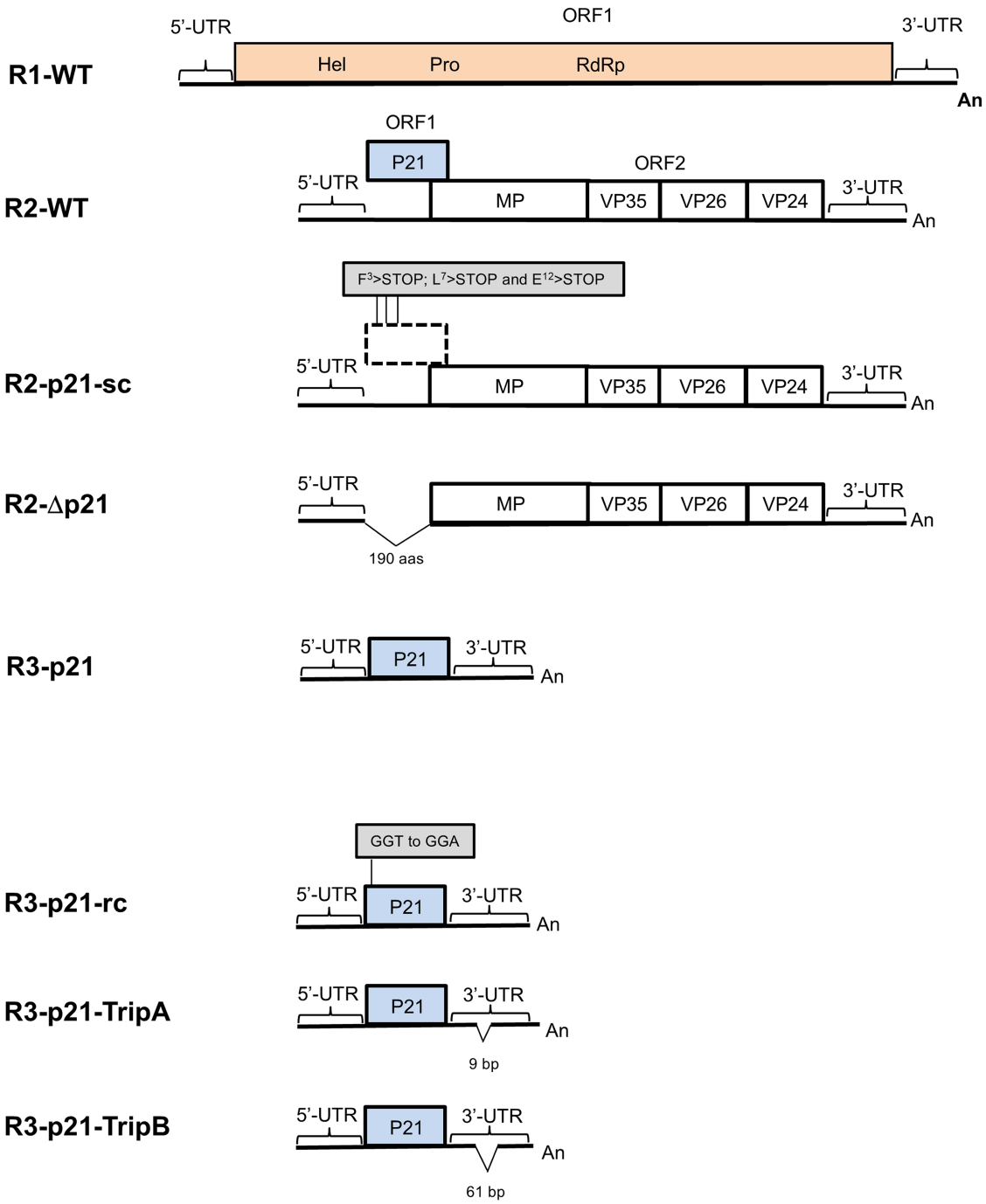

Figure 1. Constructs used in this study. Diagram showing the constructs used in this study. The construct pJL89-M-R1 (R1-WT), pJL89-M-R2 (R2-WT), and R3-p21 (Ferriol et al. 2016b) and the series of R3-p21 3′-UTR deletion mutants are shown. Horizontal lines represent the RNA genome and boxes indicate ORFs. The RNA2-encoded proteins are: RNA2-ORF1 protein (P21), movement protein (MP), and the three capsid proteins (VP35, VP26, and VP24). The 5′- and 3′-UTRs are shown as lines highlighted by a horizontal square bracket. The polyadenylated tail is shown at the 3′ end of the RNA (An). The positions of the stop codons introduced in R3-p21-sc are highlighted in a box. Details of the ToANV RNA2-derived deletion mutants are indicated.

Host range, stability, and fitness of the newly derived tripartite torradovirus

To determine whether these constructs were indeed able to immediately replicate as such without further mutations and mimic the systemic infection of the WT virus, we engineered two R3-p21-derived constructs with the deletion in the 3′-UTR region which we obtained in experiment I and experiment II (9 bp and 61 bp, respectively) and the resulting constructs were named R3-p21-TripA and R3-p21-TripB (Fig. 1). We agroinfiltrated four *N. benthamiana* plants with the two ToANV "tripartite viruses," hereafter referred as ToANV-TripA (R1-WT + R2-Δp21 + R3-p21-TripA) and ToANV-TripB (R1-WT+ R2-Δp21 + R3-p21-TripB). As a positive control we also agroinfiltrated 5 *N. benthamiana* plants with ToANV WT constructs (R1-WT + R2-WT). At 4 dpa, all plants showed typical symptoms of infection and we confirmed the presence of the three RNAs in the derived-progeny of ToANV-TripA and ToANV-TripB by northern

Table 1. Trans complementation experiments to assess the ability of a putative RNA2-ORF1 expressing construct to supplement the activity in trans of the RNA2-ORF1 knockout mutants designed in tomato apex necrosis RNA2.

Inoculated constructs[a]	Experiment	4 dpa Local[b]	4 dpa Systemic[b]	7 or 8 dpa Systemic[b]	15 or 16 dpa Systemic[b]
R1-WT+R2-WT	Exp1	2/2	2/2	2/2	N/A
	Exp2	2/2	5/5	N/A	N/A
	Exp3	N/A	13/15	15/15	15/15
R1-WT+R2-p21-sc	Exp1	2/2	0/2	0/2	0/2
	Exp2	5/5	0/5	0/5	0/5
	Exp3	N/A	N/A	0/15	0/15
R1-WT+R2-p21-sc+R3-p21	Exp1	2/2	0/2	0/2	2/2
	Exp2	5/5	0/5	0/5	5/5
	Exp3	N/A	N/A	0/15	10/15
R1-WT+R2-Δp21	Exp1	2/2	0/2	0/2	0/2
	Exp2	5/5	0/5	0/5	0/5
	Exp3	N/A	N/A	0/15	0/15
R1-WT+R2-Δp21+R3-p21	Exp1	2/2	0/2	0/2	1/2
	Exp2	5/5	0/5	0/5	1/5
	Exp3	N/A	N/A	0/15	2/15

[a]Constructs are those described in Fig. 1 and in the text.
[b]The numbers in the these columns represent the numbers of infected plants/number of tested plants present in the experiment; dpa = days post-agroinfiltration. Tests to confirm virus infection were carried out through western blot (for Exp1 and Exp2) and by DAS-ELISA for Exp3. N/A = test not carried out for the specific experiment. Local and Systemic refers to inoculated leaves and upper uninoculated leaves, respectively.

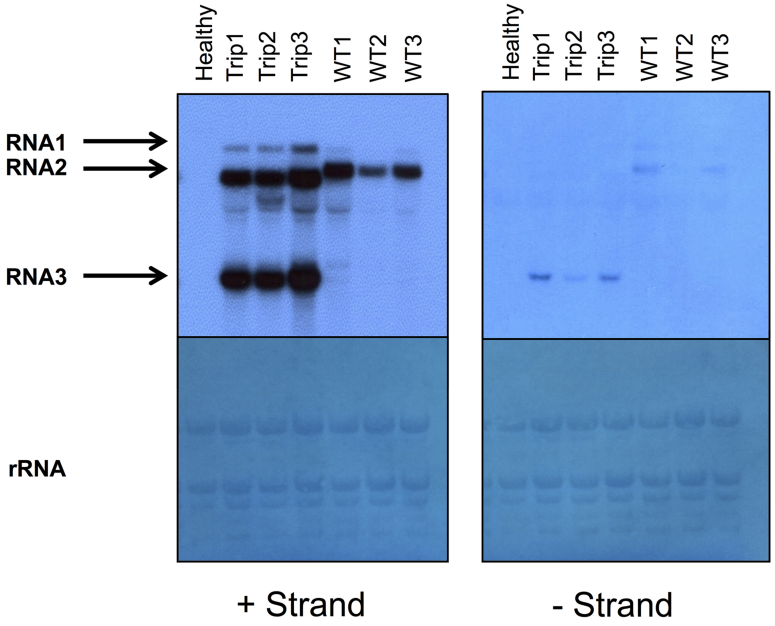

Figure 2. Attempts at complementation of a P21 deletion mutant providing P21 "*in trans*" results in systemic infection with a replicating tripartite virus. Northern blot analysis using plus-strand (left panels) and minus-strand (right panels) hybridizing probes, designed in the 3′-UTR region common to RNA1 and RNA2 of ToANV reveal that in three extracts from systemically infected plants that were inoculated with R1-WT + R2-Δp21 + R3-p21 (the samples are called Trip1, Trip2, and Trip3) we can detect both plus-strand and minus-strand RNAs corresponding to a smaller genomic RNA of the size predicted based on R3-p21 transcript size. WT1, WT2, and WT3 are lanes loaded with three samples of total RNA from plants inoculated with R1-WT + R2-WT constructs. Ribosomal RNA loading can be compared in the two bottom panels representing the same membranes of the top panels stained with methylene blue. Healthy, corresponds to total RNA extracted from mock inoculated plants. Arrows point to RNA1, RNA2, and RNA3. Note that RNA2 size in the Trip1-3 samples carries the deletion provided in the infectious clone (smaller size).

blot analyses (Fig. 4) showing that indeed only after incorporating the replication-dependent 3′-UTR region deletions, the P21 expressing construct can complement *in trans* the loss of function of RNA2 P21 knock out. Our results showed that both tripartite viruses had three replicating RNAs corresponding to their expected sizes.

Defective mutants arise many times from the populations of viruses, but the biological properties and fitness of these variants is often different from the WT virus (García-Arriaza et al. 2004). Thus, we decided to focus on one of our tripartite viruses (ToANV-TripB) and determine if its biological properties were comparable to ToANV-WT and test Koch's postulates for the ToANV-TripB. First, we compared the host range of the bipartite (ToANV-WT) and tripartite (ToANV-TripB) viruses, agroinfiltrating different hosts (Table 2). Our results showed that ToANV WT and the tripartite virus ToANV-TripB had the same biological host range for the hosts tested providing the infection through agroinfiltration. Symptoms were similar in the plant species tested except for

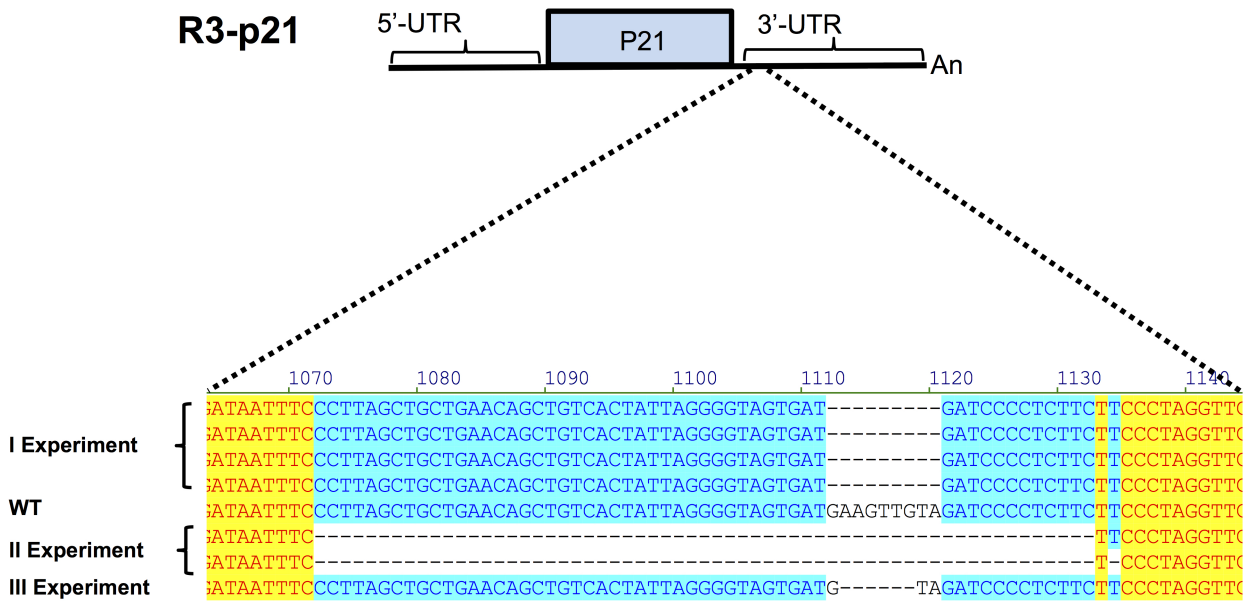

Figure 3. The third replicating RNAs in tripartite ToANVs carry specific deletions in the 3′-UTR. For each of the three complementation experiments described in Table 1 that yielded a tripartite systemic virus infection (R1-WT + R2-Δp21 + R3-p21), we performed a full-length Sanger sequence of the putative RNA3, for one systemically infected plant in each of the three experiments. Sequence alignments reveal that all three tripartite viruses carry a specific deletion in the same region of the 3′UTR, each characterized by a different size ranging from 6 to 61. Numbers in the alignment refer to the sequence of the cDNA clone provided *in trans*, schematically reproduced in the upper part of the figure. Brackets include different cDNA clones sequenced from a single systemically infected plant for each experiment. Blue indicates the location of deletions.

tomato, where systemic symptoms were milder for the tripartite virus (Supplementary Fig. S5). Second, we checked whether the ToANV-TripB was able to be maintained through several passages of mechanical inoculation. We performed 11 passages of mechanical inoculation of ToANV-TripB and as control ToANV WT in *N. benthamiana* plants and evaluated the viral progeny after these passages by northern blot analyses (Fig. 5) and next-generation sequencing (NGS) (Supplementary Tables S2 to S4). Our results showed that after 11 passages the tripartite virus ToANV-TripB was maintained in the population without major genomic rearrangements; the quasispecies sequence of these viruses passaged mechanically were determined by NGS (reads available in Sequence Read Archive accession PRJNA1126753). The whole-genomic sequences of ToANV-WT and ToANV-Trip B virus infections looking at nucleotide variants of reads mapping on the two distinct genomes with their associated reference sequences (those of the infectious clones) are displayed in Supplementary Tables S2 to S4. A number of nucleotide polymorphisms are present in specific positions, some of them appearing in all the different samples, but there is not a single specific change in RNA1 and RNA2 that is associated with the presence of a third replicating RNA.

When mechanical inoculation of ToANV-TripB was attempted from tomato plant extracts to tomato plants (susceptible cv York), we were not able to reproduce infection, showing in this case a different outcome compared to ToANV WT virus.

We then performed a competition assay by agroinfiltration of mixed infections of both viruses (ToANV-WT and ToANV-TripB) in equal amounts based on the OD values of the *A. tumefaciens* cells used for infiltration in *N. benthamiana* plants. As controls, we agroinfiltrated single infections of ToANV-WT and ToANV-TripB. Systemically infected plants were analyzed by northern blot 7 dpa to verify the possible presence of the tripartite virus together with the WT in the mixed infections. The amount of viral RNA that we detected in each systemically infected plant differed among the various replicates, but no evidence of the tripartite virus alone or in mixed infection was obtained (Fig. 5). Therefore, in a mixed infection the WT virus quickly outcompetes ToANV-TripB.

The tripartite virus yields virions that encapsidate RNA3

We then proceeded to investigate if the properties of ToANV-TripB virus were similar to ToANV WT in relationship to virion formation and RNA encapsidation. From systemically infected *N. benthamiana* plants, we harvested equal amounts of leaves and purified virions according to a protocol previously described in detail (Turina et al. 2007). After sucrose gradient centrifugation, pure virion preparations of both viruses were obtained: SDS–PAGE analysis shows the three capsid proteins present in comparable amounts between ToANV WT and ToANV-TripB purified preparations (Fig. 6a) showing that ToANV-TripB also accumulates stable virions. We then proceeded to investigate if RNA3 was also encapsidated, and not simply moved systemically as free RNA. Northern blot analysis of post sucrose gradient purified virion preparations showed the presence of RNA3 (Fig. 6b). TEM observation of the preparations showed virions of similar size and shapes with a higher percentage of stain-penetrated empty (or partially full) particles, possibly reflecting a lower affinity of the proteic components of the virion with the deleted version of the UTR in RNA3 of the tripartite virus compared to the WT 3′-UTR (Fig. 6c).

The tripartite virus can be transmitted in controlled environment by whiteflies

To verify whether the ToANV-Trip B tripartite virus is competent for whitefly transmission, we performed *T. vaporariorum*

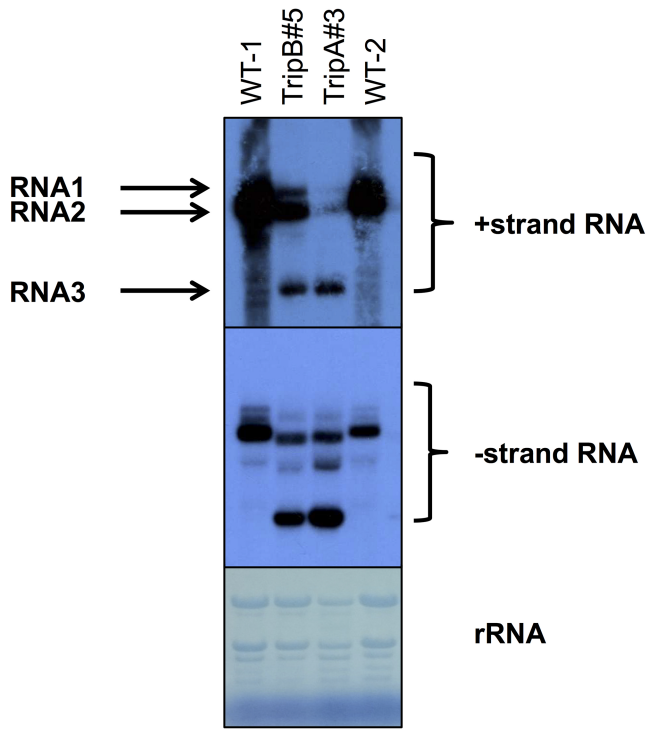

Figure 4. Agroinoculation of the artificially created tomato apex necrosis tripartite virus results in efficient systemic infection. Northern blot analysis using plus-strand (upper panel) and minus-strand (lower panel) hybridizing probes, designed for the 3′-UTR regions common to RNA1 and RNA2 of ToANV reveal that actively replicating tripartite virus can be detected in systemically infected leaves harvested 4 dpa. WT-1 and WT-2 are lanes loaded with total RNA extracts from leaves from two distinct systemically infected plants inoculated with R1-WT + R2-WT 4 days before collecting the samples. TripA#3 and TripB#5 are extracts of systemically infected plants harvested 4 dpa with the following constructs: R1-WT + R2-Δp21 + R3-p21-TripA and R1-WT + R2-Δp21 + R3-p21-TripB, respectively. Ribosomal RNA loading can be compared in the bottom panel representing the same membranes of the top panels stained with methylene blue. Arrows point to RNA1, RNA2, and RNA3. Note that RNA2 size in the TripA#3 and TripB#5 samples carry the deletion provided in the infectious clone (smaller size).

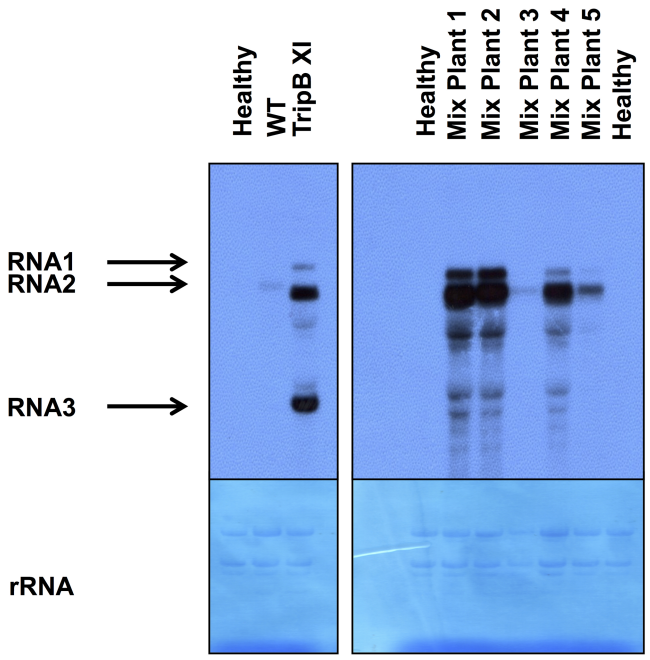

Figure 5. Tomato apex necrosis tripartite virus can be maintained through mechanical inoculation for 11 passages but is quickly overcome by the WT virus in co-inoculation experiments. The left panels display samples of *N. benthamiana* plants mechanically inoculated serially with virus obtained from WT infection (R1-WT + R2-WT) and from TripB infection (R1-WT + R2-Δp21 + R3-p21-TripB). The WT sample was collected at time of infection when recovery of symptoms occurred (20 dpi), while the TripB XI represents a sample collected at the 11th mechanical inoculation passage in a symptomatic stage (5 dpi). The right-side panels display northern blot analysis of leaf extracts from systemically infected plants harvested 7 dpa with a mix of equal amounts of *A. tumefaciens* harboring the R2-WT clone and the R2-Δp21 + R3-p21-TripB clones. Each lane is loaded with a different plant from the same experiment (Mix Plant 1 to Mix Plant 5). Northern blot was carried out using plus-strand hybridizing probes, designed in the 3′-UTR regions common to RNA1 and RNA2 of ToANV. Ribosomal RNA loading can be compared in the bottom panels representing the same membranes of the top panels stained with methylene blue. Arrows point to RNA1, RNA2, and RNA3. Healthy represents extracts from mock inoculated plants.

Table 2. Host range of plants agroinfiltrated with ToANV WT or ToANV Trip B 14 dpa.

Host	Constructs[a]	
	ToANV WT[b]	ToANV Trip B[b]
Nicotiana clevelandii	2/2	2/2
Nicotiana rustica	0/2	0/2
Nicotiana tabacum White Burley	2/2	2/2
Solanum lycopersicum cultivar York	2/2	2/2
Capsicum annuum cultivar Quadrato D'asti	0/2	0/2
Nicotiana megalosiphon	2/2	2/2
Datura stramonium	2/2	1/2
N. benthamiana	2/2	2/2
Nicotiana glutinosa	2/2	2/2
N. occidentalis	2/2	1/2

[a]Constructs agroinfiltrated in different host plants: ToANV WT (R1-WT + R2-WT) or ToANV TripB mutant (R1 + R2 R2Δp21 + R3-p21-TripB).
[b]Number of plants infected divided by the number of total plants agroinfiltrated after 14 dpa. ToANV infection was detected by DAS-ELISA carried out on extracts from the upper uninoculated leaves of different hosts.

transmission experiments of the tripartite virus using the same acquisition times and inoculation access times as in previous experiments (Ferriol et al. 2016b). We used as acquisition host *N. benthamiana* systemically infected leaves 7 dpa, whereas for inoculation we used both *N. occidentalis* and *P. floridana* plants. Using whiteflies left to acquire on WT infected leaves, we could obtain successful transmission in four out of six inoculated *N. occidentalis* plants and two out of five *P. floridana* plants. When whiteflies were left to acquire on ToANV-TripB-infected plants, two plants out of six *N. occidentalis* resulted systemically infected, whereas none of the three *P. floridana* plants were infected. We extracted RNA from a subset of plants showing systemic symptoms and a northern blot was carried out to reveal the presence and sizes of the viral RNAs (Supplementary Fig. S6): as expected the plant exposed to whitefly which had acquired from plants infected with ToANV WT RNA, accumulated a full-length RNA2, whereas the two samples extracted from plants inoculated with whiteflies which had acquired on ToANV-TripB-infected plants showed the presence of the RNA2 deleted form, and the RNA3. Overall, these results

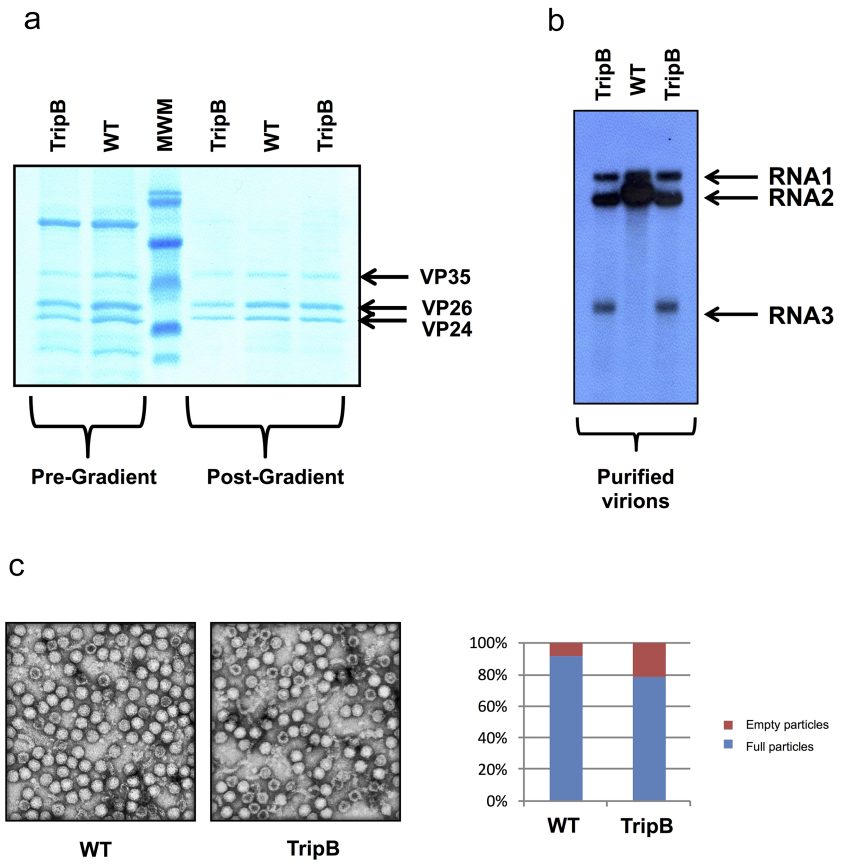

Figure 6. Tomato apex necrosis tripartite virus forms stable virions and encapsidates the third genomic RNA. Panel A displays Coomassie stained SDS–PAGE of samples from purified WT virions and TripB virus pre- and post-gradient. The arrows point at the three proteins that are present in purified virions (VP35, VP26, and VP24). MWM = molecular weight marker. Panel B displays northern blot analysis of RNA extracted from equal amount of the same virus purification displayed in panel A. Arrows in this panel point to the position of the bands representing the three genomic RNAs. Panel C displays representative pictures of virus purifications taken with the transmission electron microscope. The right-end graph shows the ratio of full and empty particles in each of the two virus purifications.

demonstrated that ToANV-TripB can be transmitted by its whitefly vector *T. vaporariorum*.

The tripartite virus can be used to generate a new GFP expressing vector able to systemically infect *N. benthamiana* plants

Previously, we have assembled a ToANV-derived vector to express GFP engineered with predicted proteolytic sites between the MP and VP35 proteins on the RNA2 (Ferriol et al. 2016b). Such vector could not be used to monitor systemic infection since GFP could only be detected in inoculated tissues and virus systemic movement was impaired. Here, based on the occurrence of the tripartite ToANV-TripB, we envisioned a new strategy to express GFP: our RNA3 expressing clone contains a second AUG just before the carboxyterminal of P21 which is the start codon of RNA2-ORF2. We, therefore, engineered a restriction site to insert in frame to this second AUG the GFP coding sequence originating the construct R3-p21-TripB-GFP (Fig. 7a), therefore, making the RNA3 bicistronic. Upon agroinfiltration of *N. benthamiana* plants with R1-WT, R2-Δp21, and R3-p21-TripB-GFP, we observed abundant GFP accumulation in the agroinfiltrated area 3 dpa, and by 6 dpa some enlarged foci in the un-inoculated leaves were also distinguishable. Also, some GFP-expressing infected leaf primordia in the germinating apex were easily distinguishable (Fig. 7b). No GFP expression was observed in the leaves corresponding to ToANV WT infection. This new tool will be pivotal in trying to fine-tune the role of specific P21 domains in long-distance spread elucidated through alanine scanning mutagenesis.

Discussion

One of the most intriguing peculiarities of members of the genus *Torradovirus* is the presence of an ORF in RNA2 upstream of the polyprotein (RNA2-ORF1, which codes for the protein P21), which is not present in other members of the family *Secoviridae*. Previously, we demonstrated that P21 protein is required for systemic infection in *N. benthamiana* and tomato plants, but not for cell-to-cell movement, virion formation, or replication (Ferriol et al. 2018). To better characterize the role of the RNA2-ORF1 protein in the infection cycle of ToANV in plants, we wanted to test if P21 is functional *in trans* on RNA2 that cannot express it. For this purpose, we provided the P21 protein "*in trans*" to two different RNA2-ORF1 mutants: one with stop codons inserted downstream of the AUG and one with an almost complete deletion of the coding sequence, R2-p21-sc and R2-Δp21, respectively. The complementation construct (R3-p21) included the intact 5′-UTR and 3′-UTR of RNA2 to possibly allow a replicative form of the construct, and not simply rely on 35S-dependent expression for P21 accumulation, which would occur without the original viral 5′- and 3′-UTRs. We have direct evidence that this construct expresses P21 protein *in vivo*, since we have previously shown by western blot analysis that the exact same construct with an engineered FLAG peptide

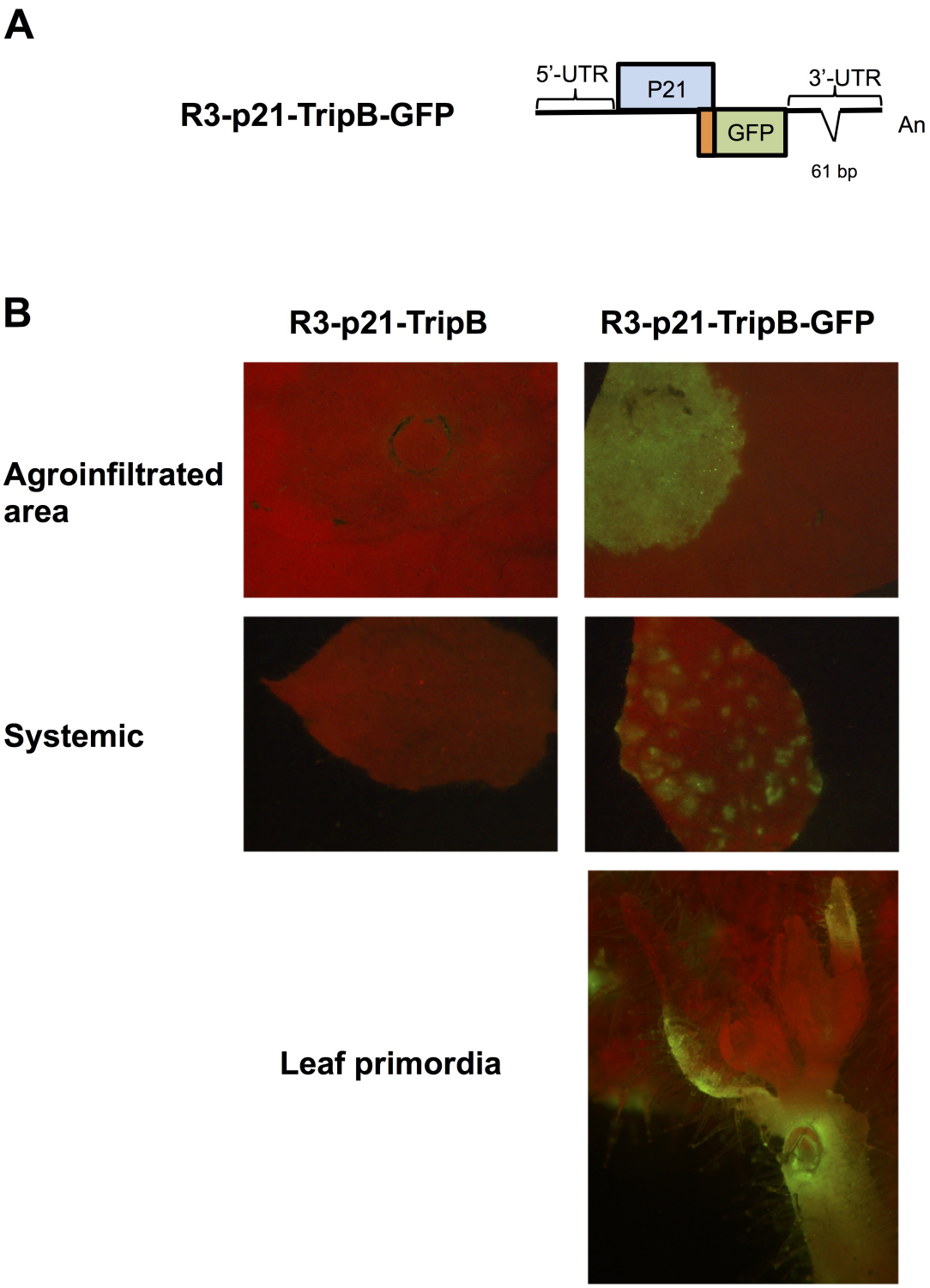

Figure 7. The tripartite construct allows to derive a new GFP viral vector able to infect *N. benthamiana* systemically. Panel A depicts the R3-p21-TripB-GFP construct showing the fusion between the initial amino acids of RNA2-ORF2 fused to GFP. Panel B displays *N. benthamiana* leaves observed under a fluorescence stereo microscope, with fluorescent light used to monitor GFP expression. Green fluorescence corresponding to GFP expression is observed both locally and systemically when the new GFP vector (R1-WT + R2-Δp21 + R3-p21-TripB-GFP, labeled as R3-p21-TripB-GFP) is agroinfiltrated in *N. benthamiana* plants. Only red chlorophyll autofluorescence can be visualized in plants agroinfiltrated with R1-WT + R2-Δp21 + R3-p21-TripB (labeled as R3-p21-TripB), used as negative control.

at the carboxy terminal accumulates the fusion protein in agroinfiltrated leaves (Ferriol et al. 2018). Agroinfiltration of R2-p21-sc in combination with R3-p21 construct resulted in a delayed yet efficient systemic infection in *N. benthamiana* plants but all the viral progeny no longer had the inserted stop codons, but had a WT sequence RNA2. We demonstrated that this change results from recombination with R3-p21-derived RNA that has an extensive region of homology in the coding region between the two

constructs. To further delineate if the RNA2-ORF1 protein could provide its function "*in trans*", we provided the R3-p21 construct in combination with R2-Δp21 construct and the outcome was the occasional (but reproducible in six experiments out of six performed) delayed infection with a tripartite virus with different types of deletions (from a minimum of 6 nt to a maximum of 61 nt) in a small region of the RNA3 3′-UTR each obtained from different plants in different experiments. Overall, our approach showed that simple expression/replication *in trans* of a third RNA expressing P21 with intact 3′-UTR does not allow immediate complementation of P21 function. *Trans*-complementation is instead restored if specific small deletions in the 3′-UTR region occurs: such deletions likely occur through local cell autonomous replication, since the mere transcription of RNA from the host RNA polymerase guided by 35S promoter would not result in >6 base long deletions (Sydow and Cramer 2009), while recombination occurring from viral replication would more easily result in the deletions we observed. Therefore, our data show that the mere local expression of the protein *in trans* does not complement the P21 defective mutants: a full complementation requires P21 expression in the context of viral replication, and in our case, such complementation requires deletions in the 3′-UTR regions for the third RNA. Only through those deletions (that we can mimic with an infectious tripartite system of clones) the system can fully recover the ability to complete the full viral infection cycle, including the ability for transmission to new host plants via whitefly. We can conclude that P21 is a trans-acting protein (a public good for a virus genome, *sensu* (Leeks et al. 2021) under specific circumstances [expression from an actively replicating segment)].

A relevant precedent to our experimental approach is the bipartitization of tobacco mosaic virus using complementing DI expressing different regions of the genome, but in that case no specific adjustment was required (or tested for), and the resulting bipartite tobamovirus was tested in plants only for local infection (Lewandowski and Dawson 2000, Knapp et al. 2005).

Another relevant example is the case of the first deconstructed virus vector assembled for cowpea mosaic virus (CPMV): in a similar approach to ours, but for the purpose of transforming CPMV in an expression vector, RNA2 was split in two defective RNAs, one coding for the MP (fused to GFP) and one coding for the CPs (L and S proteins): such vector was unstable and recombined to form a full-length RNA2, reverting to bipartite: in our case, the tripartite virus was stable and never reverted to the WT bipartite form (Verver et al. 1998).

To determine whether the deletions we observed had an effect on the secondary structure of its derived RNAs, we compared the predicted secondary RNA structure of the derived RNAs with 6-, 9-, and 61-bp deletions in the R2-p21 3′-UTRs and found out that the absence of these 9- and 61-bp deletions would change the conformation of the 3′-UTR of the derived RNAs, but not in the case of the 6-bp deletion (Supplementary Fig. S3). Deletions at the 3′-UTRs of torradoviruses have only been naturally reported for the RNA1 of the Polish tomato torradovirus isolate Kra (Budziszewska et al. 2014); nevertheless, the fact that the 6-bp deletion does not result in major changes in predicted RNA secondary structure seem to rule out the possibility that 3′-UTR conformational changes are strictly necessary for the replication of the RNA3 in the tripartite virus context. Working with secondary structures "predicted" *in silico* has many limitations, and does not generally address alternative long-range interactions within RNA molecules and between different RNA molecules. Possible long-range interactions could be at the base of the selection for small deletions in the 3′-UTR.

A possible model to explain the necessity of these deletions in the third RNA UTR for the selection of a stable tripartite virus hypothesizes a negative regulatory role of that region when it cannot interact long distance through base pairing with other regions of RNA2 that are no longer present in the R3-p21 construct (lack of possible long-range interaction would put a selective pressure on recombination bringing to the deletion of the negative regulatory element). For this reason, we tried to verify a possible long-range interaction within the RNA2 (details in Supplementary online text) deriving two constructs that would potentially allow some long-range interactions identified *in silico*. Our results with R3-p21αβγ and R3-p21βγ complementing constructs, that would allow a predicted interaction within the RNA2 that is prevented in R3-p21, has indeed identified a small region (204 nt) that confers stability to the tripartite interaction (complementation without compensatory deletions in the 3′-UTR). This is a starting point for future experimental setups that will address the significance of this region in the complex of the interaction among the three RNAs.

Another simple model that would explain the selection of small deletions in the 3′-UTR of RNA3 would suggest that having two 3′-UTR that are identical in two distinct genomic RNAs would dramatically unbalance the genome formula, favoring the shorter RNA3 to a point that would prevent sufficient RNA2 accumulation and this would results in a dead end for infectivity: it is in fact noticeable that RNA3 is always the most abundant in the tripartite viruses, and the deletions in the 3′-UTR that are selected in our tripartite viruses could be compensatory mutations to decrease to an acceptable threshold the competition with RNA2 either through lower affinity for encapsidation, or lower affinity for unidentified host factors required for replication or movement.

To investigate whether these deletions would have an effect on the biological fitness of the arisen tripartite viruses, we engineered two constructs harboring the 9- and 61-bp deletions and confirmed that the tripartite viruses were able to replicate, and quickly infect systemically *N. benthamiana* plants and cause symptoms in (4 dpa) and in one of the two cases we verified that the tripartite virus was stable in the population for the 11 serial mechanical inoculation passages we assayed. In addition, the biological host range was similar for ToANV-WT and ToANV-TripB when agroinfiltrated in different hosts. We did note that in tomato plants systemic symptoms were milder for ToANV-TripB.

The tripartite virus stochastically arisen in our artificial evolution experiment was from *N. benthamiana* plants and, a fitness cost was evident when moving this virus in tomato through mechanical inoculation as predicted by theoretical models (Elena and García-Arenal 2023): in fact, mechanical inoculation from tomato to tomato plants of TripB did not produce infection in tomato plants suggesting a fitness cost of the *N. benthamiana*-evolved TripB in tomato plants. In addition, when competition experiments of ToANV WT versus TripB in *N. benthamiana* plants were performed, the bipartite WT virus outcompetes the TripB virus, also suggesting in this host a fitness cost.

ToANV TripB was also capable of forming virions and being transmitted by its whitefly vector, and allowed the use of this tripartite virus to be engineered as a viral vector to study in the future the role of different P21 conserved motifs on torradovirus biology. The engineered viral vector was able to infect *N. benthamiana* systemically.

Transitions from monopartite to multipartite viral forms have been described *in vitro* under conditions of high multiplicity of infection (MOI) for animal viruses. Passages of foot-and-mouth disease virus in cell culture generated defective RNAs that were

infectious by complementation (García-Arriaza et al. 2004). Their demonstration indeed relied on infectious clones that split the original genome in two segments, mimicking the bipartite virus obtained *in vitro* from experimental evolution. In that case, the bipartite system had better fitness (at high MOI) because of increased particle stability of virions with smaller genomic RNA (Ojosnegros et al. 2011) contrary to what happens in our system, that has lower fitness and cannot extinguish the WT version of RNA2 in co-inoculation experiments, showing a basic difference between a natural evolutionary adaptation to multipartitism (*in vitro*) and the one forced by our experimental design through infectious clones. In another artificial evolution experimental approach, a tri-segmented bunyavirus (rift valley fever virus) was developed into a four-segmented virus that can be used as a vaccine, demonstrating the potential of artificial evolution to derive biotechnological applications (Wichgers Schreur et al. 2015).

Evolution of multipartitism is an interesting aspect of virus evolution that has received recent attention and different theoretical approaches are under experimental scrutiny. Often, modeling mathematically the natural transition from monopartitism to multipartitism takes in consideration the fact that shorter RNAs are easier to replicate, but that any non-cell autonomous element of the virus life cycle is complicated by multisegmentation, for example, requiring all the segments to be coordinately transported to neighboring cells. In the past, most scenarios for evolution of multipartitism relied on group-level benefits that allowed the evolved multipartite virus to outcompete the original monopartite ancestor (Gutiérrez and Zwart 2018, Zwart and Elena 2020) or assuming minimal conflict between genome segments (Sicard et al. 2016); a recent work suggest that a different theoretical framework (multipartitism arisen from complementing cheaters) can indeed be better suited to explain multipartitism of three or more particles/genomes (Leeks et al. 2023). Our work shows that a transition from bipartite to tripartite through the establishment of two complementing RNAs (the RNA2 that has lost P21 and the RNA3 that only encodes for P21 and has lost the ability to code for MP and CPs) does not outrun the original bipartite virus in a direct competition experiment, therefore, suggesting that for a long-term maintenance of the tripartite virus in nature some form of group level adaptation is required. Furthermore, also considering new adaptive features related to different hosts, we show that a newly engineered tri-segmented virus can evolve in a stable virus, but with lower fitness in the original host (tomato) compared to the host where the evolution occurred (*N. benthamiana*) (consider our inability to mechanically transmit serially the tripartite virus in tomato): as often mentioned in models/discussion of evolution of multipartitism, apparent loss of fitness in the original host, can allow to develop new adaptive features when moving to a different host providing new plasticity in the regulation of protein expression. Nevertheless, our results showed that a fitness cost is also present in the host where evolution occurred since direct comparison in *N. benthamiana* shows that the tripartite adapted version of ToANV is outcompeted by the WT.

Here, using knowledge derived from the tripartite adaptation studied, we provide a ToANV GFP expression vector that can infect systemically plants with a deconstructed-vector approach. Secovirid-based systems for the expression of whole genes have been based on modifications of the RNA2 and co-inoculation with unmodified RNA1 to provide the proteins required for replication and processing (Choi et al. 2019, Zarzyńska-Nowak et al. 2024). Some of the main constraints are related to: (i) genome size: by introducing non-viral sequences into the viral genome can result difficult for icosahedral viruses subjected to constraints of genome size for efficient encapsidation; (ii) duplication of cleavage sites: the cleavage sites of the encoded polyproteins have to be identified and the duplication of these cleavage sites can lead to recombination or gene products with bigger size. One of the alternatives to modify the RNA2 is creating deconstructed viruses with more than two RNA molecules. In the case of torradoviruses, two viral vectors tagged with GFP had been engineered by inserting the GFP between the MP and the coat protein VP35 and duplicating the cleavage sites, but while ToTV was successful, our ToANV failed to reproduce systemic infection (Ferriol et al. 2016b, Wieczorek et al. 2020).

In conclusion, our work shows that members of the family *Secoviridae* can potentially develop a stable tripartite genome and that no mechanistic constraints to tripartitism exist in this viral family. Nevertheless, our experimental data show that considerable fitness costs come with the stable tripartite virus we have generated through engineering and evolution, which could explain why this family is represented only by monopartite and bipartite genomes.

Finally, the results obtained in this work are important to understand the role of the P21 protein in the infection cycle of torradoviruses. We foresee the use of the engineered viral vector to study the still unresolved molecular and biochemical properties of P21 in the torradoviruses infectious cycle.

Acknowledgements

We also would like to acknowledge the technical support of Riccardo Lenzi. We would like to acknowledge the invaluable contributions of two anonymous reviewers. Their constructive criticism and insightful suggestions significantly enhanced the quality of the final manuscript.

Author contributions

Conceptualization: M.T., I.F; funding acquisition: M.T., I.F., B.F; writing—review and editing: M.T., I.F., B.F., M.C., M.V., L.N; writing—original draft: M.T. and I.F; data curation: L.N; investigation methodology: M.C., M.V., M.T., I.F., N.M., M.F.

Supplementary data

Supplementary data is available at *VEVOLU Journal* online.

Conflict of interest: None delcared.

Funding

This research was partially funded by Grant SCB11058 from the California Department of Food and Agriculture (CDFA), United States.

Data availability

Raw reads from the Illumina sequencing are available upon request.

References

Bertran A, Ciuffo M, Margaria P *et al.* Host-specific accumulation and temperature effects on the generation of dimeric viral RNA species derived from the S-RNA of members of the Tospovirus genus. *Journal of General Virology* 2016;**97**:3051–3062.

Bonnamy M, Brousse A, Pirolles E *et al.* The genome formula of a multipartite virus is regulated both at the individual segment and the segment group levels. *PLoS Pathog* 2024;**20**:e1011973.

Budziszewska M, Wieczorek P, Zhang Y *et al*. Genetic variability within the polish tomato torrado virus Kra isolate caused by deletions in the 3′-untranslated region of genomic RNA1. *Virus Res* 2014;**185**:47–52.

Choi B, Kwon S-J, Kim M-H *et al*. A plant virus-based vector system for gene function studies in pepper. *Plant Physiol* 2019;**181**:867–80.

Crivelli G, Ciuffo M, Genre A *et al*. Reverse genetic analysis of ourmiaviruses reveals the nucleolar localization of the coat protein in *Nicotiana benthamiana* and unusual requirements for virion formation. *J Virol* 2011;**85**:5091–104.

Dall'Ara M, Guo Y, Poli D *et al*. Analysis of the relative frequencies of the multipartite BNYVV genomic RNAs in different plants and tissues. *J Gen Virol* 2024;**105**:001950.

Edgar RC, Taylor B, Lin V *et al*. Petabase-scale sequence alignment catalyses viral discovery. *Nature* 2022;**602**:142–47.

Elena SF, García-Arenal F. Plant virus adaptation to new hosts: a multi-scale approach. In: Domingo E, Schuster P and Elena SF *et al*. (eds), *Viral Fitness and Evolution. Current Topics in Microbiology and Immunology*, Vol. **439** pp.167–196. Cham: Springer, 2023.

Ferriol I, Silva Junior DM, Nigg JC *et al*. Identification of the cleavage sites of the RNA2-encoded polyproteins for two members of the genus Torradovirus by N-terminal sequencing of the virion capsid proteins. *Virology* 2016a;**498**:109–15.

Ferriol I, Turina M, Zamora-Macorra EJ *et al*. RNA1-independent replication and GFP expression from tomato marchitez virus isolate M cloned cDNA. *Phytopathology* 2016b;**106**:500–09.

Ferriol I, Vallino M, Ciuffo M *et al*. The torradovirus-specific RNA2-ORF1 protein is necessary for plant systemic infection. *Mol Plant Pathol* 2018;**19**:1319–31.

Fuchs M, Bar-Joseph M, Candresse T *et al*. ICTV virus taxonomy profile: *Closteroviridae*. *J Gen Virol* 2020;**101**:364–65.

Fuchs M, Hily J-M, Petrzik K *et al*. ICTV virus taxonomy profile: *Secoviridae* 2022. *J Gen Virol* 2022;**103**:1807.

García-Arriaza J, Manrubia SC, Toja M *et al*. Evolutionary transition toward defective RNAs that are infectious by complementation. *J Virol* 2004;**78**:11678–85.

Gutiérrez S, Zwart MP. Population bottlenecks in multicomponent viruses: first forays into the uncharted territory of genome-formula drift. *Curr Opin Virol* 2018;**33**:184–90.

Johnson PZ, Kasprzak WK, Shapiro BA *et al*. RNA2Drawer: geometrically strict drawing of nucleic acid structures with graphical structure editing and highlighting of complementary subsequences. *RNA Biol* 2019;**16**:1667–71.

Knapp E, Danyluk GM, Achor D *et al*. A bipartite tobacco mosaic virus-defective RNA (dRNA) system to study the role of the N-terminal methyl transferase domain in cell-to-cell movement of dRNAs. *Virology* 2005;**341**:47–58.

Leeks A, West SA, Ghoul M. The evolution of cheating in viruses. *Nat Commun* 2021;**12**:6928.

Leeks A, Young PG, Turner PE *et al*. Cheating leads to the evolution of multipartite viruses. *PLoS Biol* 2023;**21**:e3002092.

Lewandowski DJ, Dawson WO. Functions of the 126- and 183-kDa proteins of tobacco mosaic virus. *Virology* 2000;**271**:90–98.

Li H, Durbin R. Fast and accurate short read alignment with burrows–wheeler transform. *Bioinformatics* 2009;**25**:1754–60.

Li H, Handsaker B, Wysoker A *et al*. The sequence alignment/map format and SAMtools. *Bioinformatics* 2009;**25**:2078–79.

Lucía-Sanz A, Manrubia S. Multipartite viruses: adaptive trick or evolutionary treat? *Npj Syst Biol Appl* 2017;**3**:34.

Mann KS, Chisholm J, Sanfaçon H. Strawberry mottle virus (family *Secoviridae*, order Picornavirales) encodes a novel glutamic protease to process the RNA2 polyprotein at two cleavage sites. *J Virol* 2019;**93**:10–1128.

Michalakis Y, Blanc S. The curious strategy of multipartite viruses. *Annu Rev Virol* 2020;**7**:203–18.

Moya A, Domingo E, Holland JJ. RNA viruses: a bridge between life and artificial life. In: *European Conference on Artificial Life*. pp.170–78. Berlin, Heidelberg: Springer, 1995.

Neri U, Wolf YI, Roux S *et al*. Expansion of the global RNA virome reveals diverse clades of bacteriophages. *Cell* 2022;**185**:4023–37.

Ojosnegros S, Garcia-Arriaza J, Escarmis C *et al*. Viral genome segmentation can result from a trade-off between genetic content and particle stability. *PLoS Genet* 2011;**7**:e1001344.

Pagnoni S, Oufensou S, Balmas V *et al*. A collection of Trichoderma isolates from natural environments in Sardinia reveals a complex virome that includes negative-sense fungal viruses with unprecedented genome organizations. *Virus Evol* 2023;**9**:vead042.

Rastgou M, Habibi MK, Izadpanah K *et al*. Molecular characterization of the plant virus genus Ourmiavirus and evidence of inter-kingdom reassortment of viral genome segments as its possible route of origin. *J Gen Virol* 2009;**90**:2525.

Sanfaçon H, Wellink J, Le Gall O *et al*. Secoviridae: a proposed family of plant viruses within the order picornavirales that combines the families Sequiviridae and Comoviridae, the unassigned genera Cheravirus and Sadwavirus, and the proposed genus torradovirus. *Arch Virol* 2009;**154**:899–907.

Sicard A, Michalakis Y, Gutiérrez S *et al*. The strange lifestyle of multipartite viruses. *PLoS Pathog* 2016;**12**:e1005819.

Sicard A, Pirolles E, Gallet R *et al*. A multicellular way of life for a multipartite virus. *eLife* 2019;**8**:e43599.

Sicard A, Yvon M, Timchenko T *et al*. Gene copy number is differentially regulated in a multipartite virus. *Nat Commun* 2013;**4**:2248.

Sydow JF, Cramer P. RNA polymerase fidelity and transcriptional proofreading. *Curr Opin Struct Bio* 2009;**19**:732–39.

Thorvaldsdóttir H, Robinson JT, Mesirov JP. Integrative Genomics Viewer (IGV): high-performance genomics data visualization and exploration. *Briefings Bioinf* 2013;**14**:178–92.

Turina M, Ricker MD, Lenzi R *et al*. A severe disease of tomato in the Culiacan area (Sinaloa, Mexico) is caused by a new picorna-like viral species. *Plant Dis* 2007;**91**:932–41.

Verver J, Wellink J, Van Lent J *et al*. Studies on the movement of cowpea mosaic virus using the jellyfish green fluorescent protein. *Virology* 1998;**242**:22–27.

Wichgers Schreur PJ, Kant J, van Keulen L *et al*. Four-segmented Rift Valley fever virus induces sterile immunity in sheep after a single vaccination. *Vaccine* 2015;**33**:1459–64.

Wieczorek P, Budziszewska M, Frąckowiak P *et al*. Development of a new tomato torrado virus-based vector tagged with GFP for monitoring virus movement in plants. *Viruses* 2020;**12**:1195.

Zarzyńska-Nowak A, Minicka J, Wieczorek P *et al*. Development of stable infectious cDNA clones of tomato black ring virus tagged with green fluorescent protein. *Viruses* 2024;**16**:125.

Zuker M. Mfold web server for nucleic acid folding and hybridization prediction. *Nucleic acids research* 2003;**31**:3406–3415.

Zwart MP, Elena SF. Modeling multipartite virus evolution: the genome formula facilitates rapid adaptation to heterogeneous environments. *Virus Evol* 2020;**6**:veaa022.

Virus Evolution, 2024, 10(1), veae098 , DOI: https://doi.org/10.1093/ve/veae098, Advance Access Publication 20 November 2024, Research Article